

Supporting information for “Modeling Blue to UV Upconversion in β -NaYF₄: Tm³⁺”

*Pedro Villanueva-Delgado,^{*a} Karl W. Krämer,^a Rafael Valiente,^b
Mathijs de Jong,^c and Andries Meijerink^c*

^aDepartment of Chemistry and Biochemistry, University of Bern, 3012 Bern, Switzerland

* pedro.villanueva@dcb.unibe.ch

^bDepartamento de Física Aplicada, Facultad de Ciencias, Universidad de Cantabria-IDIVAL, 39005 Santander, Spain.

^cCondensed Matter and Interfaces, Debye Institute for Nanomaterials Science, Utrecht University, 3508TA Utrecht, The Netherlands.

Powder X-ray diffraction

Powder X-ray diffractograms of the β -NaYF₄: Tm³⁺ samples are shown in Fig. S1. The diffraction patterns were measured on a Stoe STADI P diffractometer in Bragg-Brentano (reflection) geometry at room temperature with Cu K α_1 radiation from a focusing α -quartz (101) monochromator. The patterns corresponds to the pure hexagonal β -NaYF₄ phase which crystallizes in space group $P\bar{6}$. The trivalent rare earth sites with C₁ and C_{3h} symmetry are randomly occupied by the Y³⁺ and Tm³⁺ ions.

Figure S1 also shows the calculated Bragg positions for space group $P\bar{6}$ and lattice parameters $a = 5.9734 \text{ \AA}$ and $c = 3.5296 \text{ \AA}$.

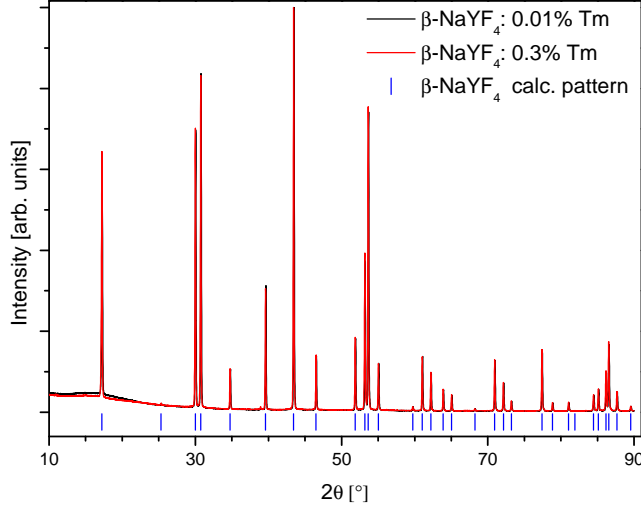


Figure S1: Powder X-ray diffractograms of β -NaYF₄: 0.01% Tm³⁺ (black line) and β -NaYF₄: 0.3% Tm³⁺ (red line). The calculated Bragg positions for space group $P\bar{6}$ and lattice parameters $a = 5.9734 \text{ \AA}$ and $c = 3.5296 \text{ \AA}$ are shown as blue ticks.

Emission

Figure S2 shows a comparison of the emission band at 6800 cm^{-1} under ${}^3\text{H}_6 \rightarrow {}^1\text{G}_4$ (at 21140 cm^{-1}) and ${}^3\text{H}_6 \rightarrow {}^3\text{H}_4$ (at 12547 cm^{-1}) excitations. The shape of both emission bands is very similar at the high energy side, but different at the low energy side. Decay curves have been recorded for different peaks of the band. The high energy side is assigned to the ${}^3\text{H}_4 \rightarrow {}^3\text{F}_4$ transition because it is present at both excitation wavelengths and the decay curves show a rise and decay that corresponds to the ${}^3\text{H}_4$ state. The low energy side shows additional peaks under ${}^1\text{G}_4$ excitation. Their decay curves are double exponentials with lifetimes corresponding to the ${}^1\text{G}_4$ and ${}^3\text{H}_4$ states, thus they are assigned to the ${}^1\text{G}_4 \rightarrow {}^3\text{F}_3$ transition. The intensity of the latter transition is lower than of the former.

Lifetimes

Intrinsic Decay Curves

The intrinsic decay curves of the ${}^1\text{D}_2$, ${}^1\text{G}_4$, and ${}^3\text{H}_4$ states are shown in Figure S3. They were recorded for the β -NaYF₄: 0.01% Tm³⁺ sample under low power excitation.

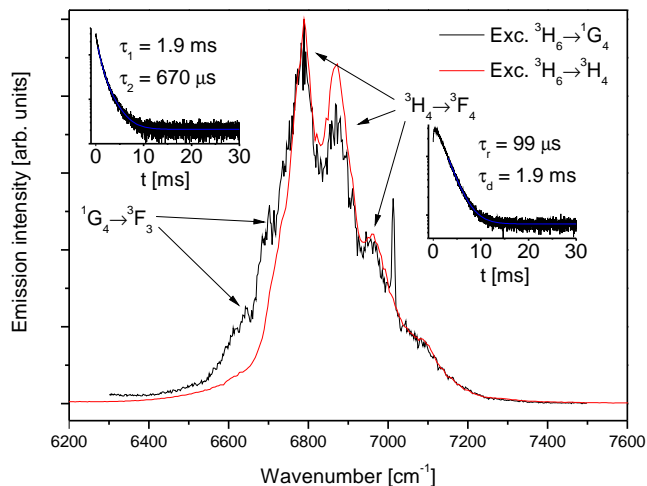


Figure S2: Comparison of the emission band at 6800 cm^{-1} under two different excitation conditions: ${}^3\text{H}_6 \rightarrow {}^1\text{G}_4$ (at 21140 cm^{-1}) and ${}^3\text{H}_6 \rightarrow {}^3\text{H}_4$ (at 12547 cm^{-1}). The band is assigned to the ${}^3\text{H}_4 \rightarrow {}^3\text{F}_4$ and ${}^1\text{G}_4 \rightarrow {}^3\text{F}_3$ transitions based on the lifetimes of the individual peaks in the band. The high energy side shows rise and decay times similar to the ${}^3\text{H}_4$ state. The low energy side decay curves are double exponentials with lifetimes similar to the ${}^3\text{H}_4$ (τ_1) and ${}^1\text{G}_4$ (τ_2) states, see Table 1.

Decay Curves under Blue Excitation

Figure S4 shows all decay curves of the emissions from the ${}^1\text{G}_4$ and ${}^3\text{H}_4$ states under 21140 cm^{-1} (473 nm) excitation of the ${}^1\text{G}_4$ state. The emissions from the same state have the same lifetime, as expected. The ${}^1\text{G}_4 \rightarrow {}^3\text{H}_5$ emission (numbered 6 in Figure 1 in the main text) overlaps the ${}^3\text{H}_4 \rightarrow {}^3\text{H}_6$ emission; therefore, its lifetime is slightly longer. The spikes at the beginning of some of the decay curves are artifacts due to the excitation pulse not being completely removed by the monochromator; they are especially noticeable for the ${}^1\text{G}_4 \rightarrow {}^3\text{H}_6$ and ${}^3\text{H}_4 \rightarrow {}^3\text{H}_6$ decays.

Two-color excitation

Figure S5 shows the pump and probe two-color excitation spectra for the ${}^1\text{D}_2 \rightarrow {}^3\text{H}_6$ emission at 27700 cm^{-1} (361 nm). The first excitation laser is fixed at 21140 cm^{-1} (473 nm) to pump the ${}^3\text{H}_6 \rightarrow {}^1\text{G}_4$ transition, The second excitation is scanned from 8000 to 6000 cm^{-1} to probe the ${}^1\text{G}_4 \rightarrow {}^1\text{D}_2$ transition. There is no relative delay between the pump and probe pulses, i.e., they arrive at the sample at the same time. The only peak at 6765 cm^{-1} corresponds to the

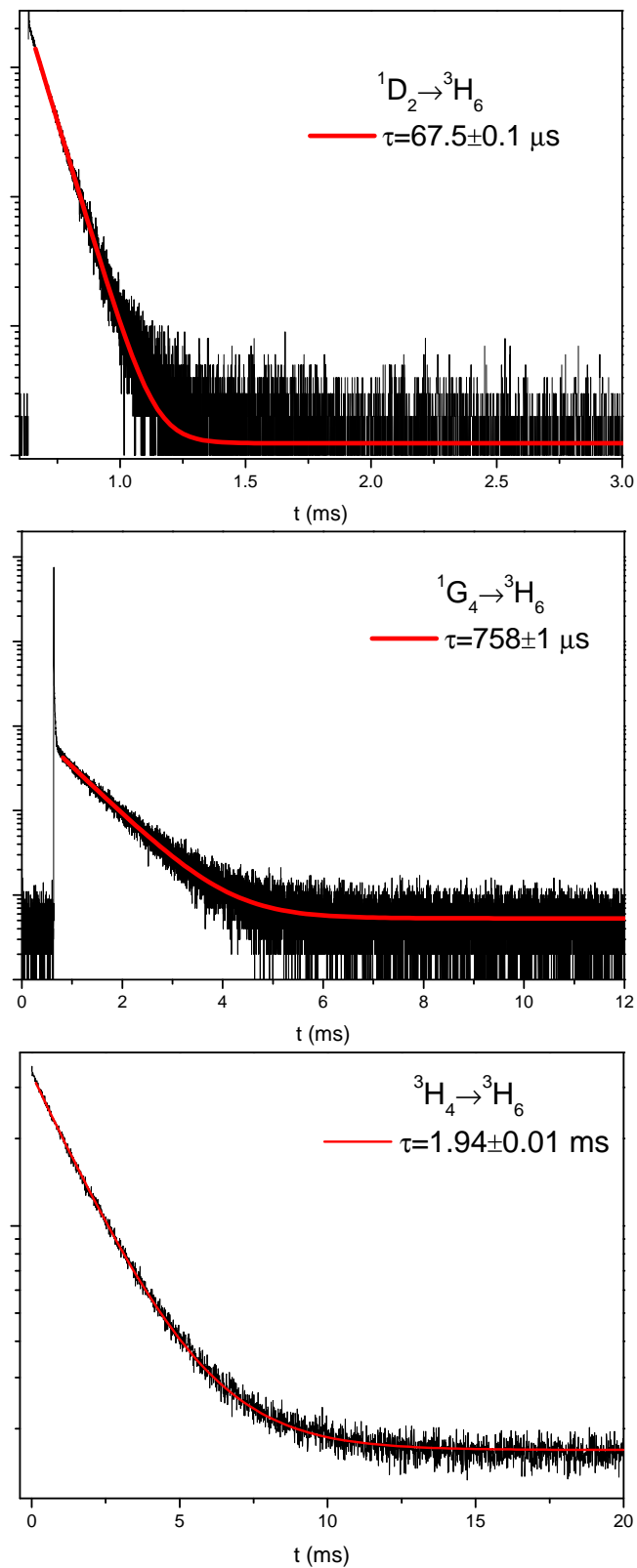


Figure S3: Intrinsic decay curves (black lines) of the 1D_2 , 1G_4 , and 3H_4 states in $\beta\text{-NaYF}_4$: 0.01% Tm^{3+} under low power direct excitation of each state. The red lines show single exponential fits to the data. The resulting lifetimes are shown in the figures.

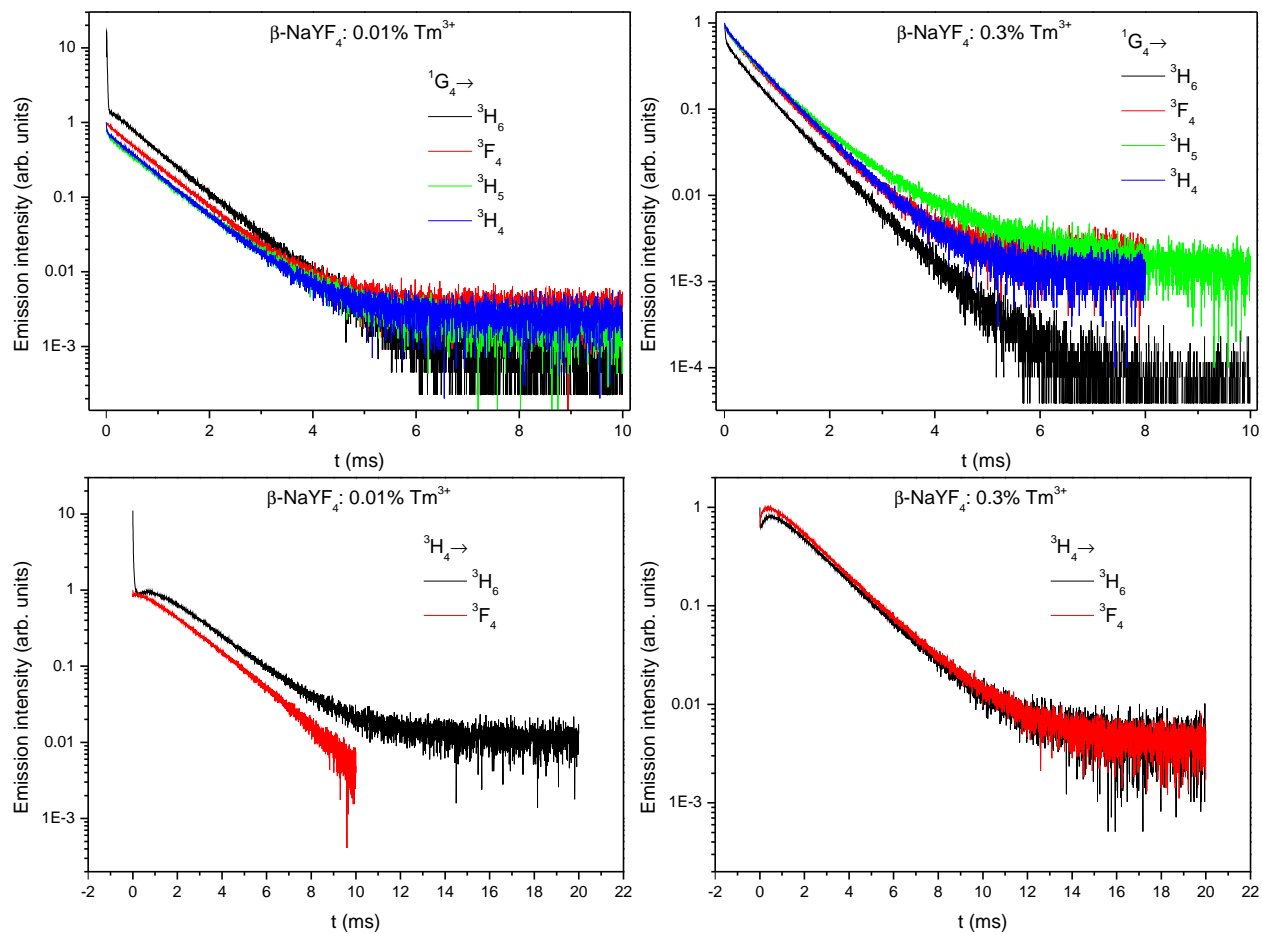


Figure S4: Decay curves of the emissions from the $^1\text{G}_4$ and $^3\text{H}_4$ states under 21140 cm^{-1} (473 nm) excitation of the $^1\text{G}_4$ state.

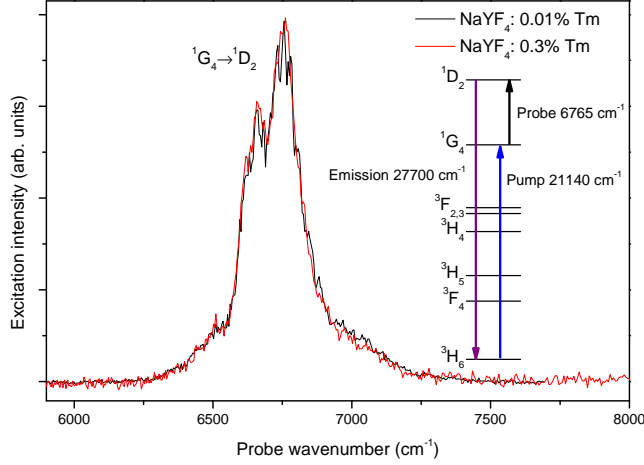


Figure S5: Pump and probe two-color excitation spectra for the ${}^1D_2 \rightarrow {}^3H_6$ emission at 27700 cm^{-1} (361 nm). The pump laser was fixed at 21140 cm^{-1} (473 nm) to pump the ${}^3H_6 \rightarrow {}^1G_4$ transition. The probe beam was scanned from 8000 to 5900 cm^{-1} to monitor the ${}^1G_4 \rightarrow {}^1D_2$ excited state absorption. There is no relative time delay between the pump and probe excitation laser pulses.

transition ${}^1G_4 \rightarrow {}^1D_2$ (i.e. the excited state absorption from 1G_4) and has the same position and shape for both samples.

Absorption

Figure S6 shows the polarization-averaged absorption spectrum of a $\beta\text{-NaGdF}_4$: $5\% \text{ Yb}^{3+}$, $0.3\% \text{ Tm}^{3+}$ single crystal at room temperature. Here we use the $\beta\text{-NaGdF}_4$ host material instead of $\beta\text{-NaYF}_4$ because of its more facile crystal growth. Both materials have the same crystal structure. The spectroscopic properties of Tm^{3+} are very similar in both lattices.

The strongest absorption band around 10200 cm^{-1} is assigned to the $\text{Yb}^{3+} {}^2F_{7/2} \rightarrow {}^2F_{5/2}$ transition. All the other bands correspond to Tm^{3+} f-f transition from the ground state 3H_6 to the excited states labeled in Figure S6. At wavenumbers higher than 30000 cm^{-1} the spectrum is dominated by Gd^{3+} absorptions from the ground state to the 6P_J , 6I_J , and 6D_J multiplets, and hence the Tm^{3+} absorption to the 3P_J and 1I_6 multiplets is obscured (data not shown). The polarization-averaged absorption cross-section of the ${}^3H_6 \rightarrow {}^1G_4$ transition at 21140 cm^{-1} is $\sigma = 7.77 \times 10^{-22} \text{ cm}^2$.

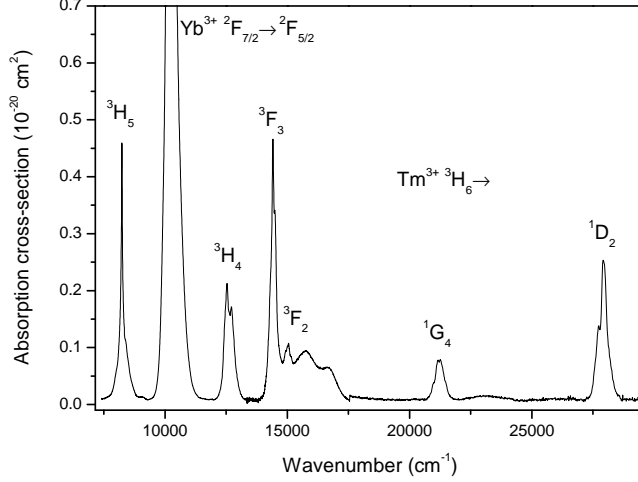


Figure S6: Room-temperature polarization-averaged absorption spectrum of a β -NaGdF₄: 5% Yb³⁺, 0.3% Tm³⁺ single crystal. All transitions originate from the ³H₆ ground state of Tm³⁺, except for the Yb³⁺ ²F_{7/2} → ²F_{5/2} transition around 10200 cm⁻¹.

Table S1: Results for the Inokuti–Hirayama model fit for the ¹G₄ → ³F₄ emission in β -NaYF₄: 0.3% Tm³⁺, see Figure S7. χ_{red}^2 is the reduced chi-square error of the fit.

n	χ_{red}^2 (10^{-6})	τ (μ s)	γ	$C_{SA}(\text{\AA}^n \text{s}^{-1})$	R_c (\AA)
6	6.77	841±2	0.513±0.003	3.2×10^9	11.80
8	6.85	767±1	0.433±0.003	5.5×10^{11}	11.97
10	7.72	736±1	0.411±0.003	2.0×10^{14}	13.10

The Inokuti–Hirayama model

The fitted parameters of the Inokuti–Hirayama model are given in **Table S1**, see also Figure S7.

The data in Figure S7 has also been fitted using the Burshtein, Zusman, and Yokota–Tanimoto models. These models introduce energy migration among the sensitizers in addition to the sensitizer-activator ET. For all these models the fit results in zero or negligible energy migration. The resulting parameters are: $W_{ET} = 0.0 \pm 0.6 \text{ s}^{-1}$ for Burshtein’s average energy migration rate, $\tau_h = 11 \pm 3 \text{ ms}$ for Zusman’s hopping time (much longer than the ¹G₄ lifetime) and $D = 0.000 \pm 0.001 \text{ cm}^2 \text{ s}^{-1}$ for Yokota–Tanimoto’s diffusion constant.

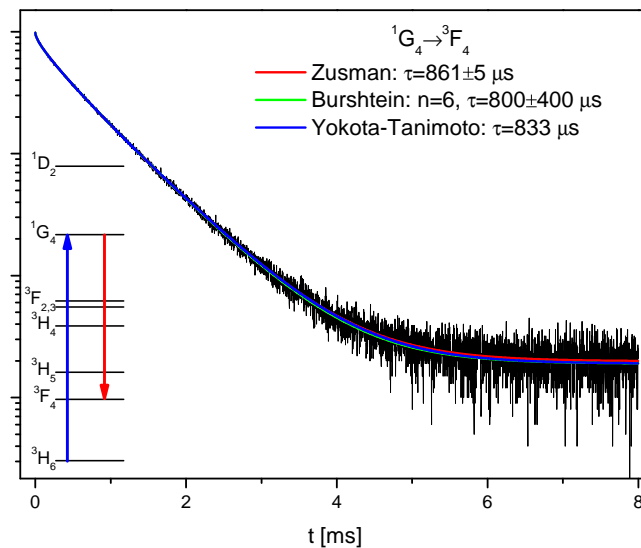


Figure S7: Decay of the 1G_4 state (black line) in $\beta\text{-NaYF}_4: 0.3\% \text{Tm}^{3+}$ with Burshtein, Zusman, and Yokota-Tanimoto fits that include energy migration.

Microscopic rate equation model

The parameters and normalized root-mean-square deviation for Scheme I and Scheme II are given in Table S2 and Table S3, respectively, for different combinations of multiplicities. The convergence of the normalized root-mean-square deviation as a function of the number of simulated ions is given in Table S4 for the optimum case of Scheme I with $n = 6$ for ETU and CR.

Table S2: Parameters and normalized root-mean-square deviation ϵ for Scheme I (ETU and CR processes) for different interaction multiplicities n . The units of the parameters depend on n .

Process	n	ϵ	Value ($\text{\AA}^n \text{s}^{-1}$)	R_c (\AA)
ETU	6	0.49	1.258×10^{10}	16.97
CR	6		4.205×10^9	12.14
ETU	6	0.99	1.301×10^9	11.63
CR	8		5.573×10^9	6.73
ETU	6	1.3	8.344×10^6	5.01
CR	10		7.491×10^9	4.74
ETU	8	1.5	2.001×10^{10}	8.86
CR	6		2.515×10^7	5.17
ETU	8	0.71	2.089×10^9	6.68
CR	8		2.683×10^{10}	8.19
ETU	8	1.4	1.111×10^8	4.63
CR	10		4.990×10^9	4.55
ETU	10	1.5	2.023×10^{10}	5.73
CR	6		2.022×10^7	4.99
ETU	10	0.83	7.400×10^{16}	25.99
CR	8		1.647×10^{10}	7.71
ETU	10	1.4	9.127×10^{11}	8.39
CR	10		4.380×10^9	4.49

Table S3: Parameters and normalized root-mean-square deviation ϵ for Scheme II (ETU and MPR) for different interaction multiplicities n . The units of the parameter depend on n .

Process	n	ϵ	Value ($\text{\AA}^n \text{s}^{-1}$)	R_c (\AA)	k_{MPR} (s^{-1})
ETU	6	0.68	1.605×10^{13}	47.98	3.263×10^8
ETU	8	1.0	3.602×10^{12}	15.12	3.309×10^8
ETU	10	1.1	3.813×10^{13}	11.12	3.356×10^8

Table S4: Normalized root-mean-square deviation ϵ and simulation time for different number of unit cells and ions. The optimum Scheme I parameters were used.

Num. unit cells	Num. ions	Simulation time (s)	ϵ
20	30	0.93	1.2
30	120	2.95	0.73
40	253	15.27	0.50
50	571	87.31	0.50
60	952	219.14	0.50
70	1463	383.44	0.54
80	2243	691.33	0.55
90	3324	1304.46	0.52
100	4569	2240.34	0.56
110	5784	2134.63	0.50